Surface & Coatings Technology 285 (2016) 203–213

Contents lists available at ScienceDirect

Surface & Coatings Technology

journal homepage: www.elsevier.com/locate/surfcoat

Evaluating mechanical properties and crack resistance of CrN, CrTiN, CrAlN and CrTiAlN coatings by nanoindentation and scratch tests

Qianzhi Wang [a], Fei Zhou [b,c,d,*], Jiwang Yan [a,**]

[a] Department of Mechanical Engineering, Faculty of Science and Technology, Keio University, Yokohama 2238522, Japan
[b] State Key Laboratory of Mechanics and Control of Mechanical Structures, Nanjing University of Aeronautics and Astronautics, Nanjing 210016, China
[c] College of Mechanical and Electrical Engineering, Nanjing University of Aeronautics and Astronautics, Nanjing 210016, China
[d] Jiangsu Key Laboratory of Precision and Micro-Manufacturing Technology, Nanjing 210016, China

ARTICLE INFO

Article history:
Received 2 September 2015
Revised 20 October 2015
Accepted in revised form 22 November 2015
Available online 1 December 2015

Keywords:
Cr-Ti-Al-N
Topic:
Nanoindentation
Crack
Residual stress
Fracture toughness.

ABSTRACT

CrN, CrTiN, CrAlN and CrTiAlN coatings were deposited on Si (100) wafers, and their microstructure, mechanical properties, fracture toughness and adhesive strength were investigated via X-ray diffraction (XRD), nanoindentation and micro-scratch tests. Besides an F.C.C. crystal structure, $TiN_{0.3}$ (004) and AlN (222) phases were found in the CrTiN and CrAlN coatings while the crystallinity of the CrTiAlN coating decreased. The hardness of the CrN (14.5 GPa), CrTiN (13.9 GPa) and CrAlN (17.7 GPa) coatings was determined by their grain sizes while the CrTiAlN coating with the most compact morphology exhibited the highest hardness of 22.0 GPa. In addition, CrTiN (K_{Ic} = 2.73 MPa·$\sqrt{m}$), CrAlN (K_{Ic} = 2.70 MPa·$\sqrt{m}$) and CrTiAlN coatings showed a stronger crack resistance than the CrN coating (K_{Ic} = 1.06 MPa·$\sqrt{m}$), especially the CrTiAlN coating without any radial cracks. However, the CrTiAlN coating encountered circumferential cracks and premature delamination (Adhesive energy G_c = 70 J/m^2) because of its highest compressive stress (4.64 GPa). Based on the results here, it is concluded that a decent compressive stress of 3.0 GPa is expected to help thin films prevent from radial and circumferential cracks simultaneously.

1. Introduction

With a growing demand of anti-wear and anti-oxidation coatings, ternary CrAlN and CrTiN, based on binary CrN coatings, have attracted intensive concerns from academics. Owing to short inter-atomic distance, small crystal and dense Al_2O_3 films, CrAlN coatings present high hardness, superior tribological properties and strong oxidation resistance [1–3]. Likewise, CrTiN coatings exhibit an enhancement in hardness and wear resistance because of the solid solution effect and the formation of TiN nanocrystal [4–6]. Subsequently, researchers devoted themselves to the studies of CrTiAlN coatings due to the merits of CrAlN and CrTiN coatings. It turns out that CrTiAlN coatings have a high hardness (30–38 GPa) and exhibit favorable anti-wear and anti-corrosion performance [7–10].

So far, many works have been done to investigate the mechanical and tribological properties of CrAlN, CrTiN or CrTiAlN coatings separately [11–18]. Namely, a comprehensive comparison of their mechanical properties in one paper is still missing in the current literature. Thus, it is unclear which element incorporation (Ti, Al or Ti–Al) is more beneficial to the mechanical properties of CrN coatings only based on the current data in Table 1. More importantly, the evolution of the crack resistance, as another form of anti-wear ability, as well as the adhesive strength amongst CrN, CrTiN, CrAlN and CrTiAlN coatings, has never been studied. Thus, it is of paramount importance to evaluate their crack resistance and adhesive ability for some more details in micro-scale, which will provide a decent prediction of their tribological properties.

In this study, CrN, CrTiN, CrAlN and CrTiAlN coatings were deposited on Si (100) wafers using closed-field unbalanced magnetron sputtering. Their crack resistances and adhesive energies were assessed via high-load (1000 mN) nanoindentation and micro-scratch tests. Accordingly, the individual fracture toughness was given, and the correlation between their mechanical properties, residual stress, adhesive strength and crack resistance was subsequently elucidated.

2. Experimental details

2.1. Coatings fabrication

Si (100) wafers (H_s = 12.4 GPa, E_s = 198 GPa, t_s = 525 ± 20 μm), as substrates, were ultrasonically washed in ethanol for 10 min before being mounted on the turning stage. When the chamber was evacuated to a pressure of 4.0 × 10^{-4} Pa, a 30-minute Ar^+ bombardment was adopted to remove contaminants and activate surface followed by a Cr

* Corresponding author. Tel.: +86 25 8489 3083; fax: +86 25 8489 3083.
** Corresponding author. Tel.: +81 45 566 1445; fax: +81 45 566 1495.
E-mail addresses: fzhou@nuaa.edu.cn (F. Zhou), yan@mech.keio.ac.jp (J. Yan).

http://dx.doi.org/10.1016/j.surfcoat.2015.11.040
0257-8972/

Table 1
Mechanical and tribological properties of CrTiN and CrAlN coatings in previous literature.

References	Method	Substrate	Ti or Al (at.%)	Hardness (GPa)	Load (N)	Velocity (m/s)	Counterpart	Friction coefficient	Wear rate (mm^3/Nm)
CrTiN									
Zeng et al. [4]	Unbalanced magnetron sputtering	HSS	15.80	39.2	2.5	0.200	Al_2O_3	0.50	4.16×10^{-7}
Zhang et al. [6]	Mid-frequency magnetron sputtering	Si (111)	16.18	–	1.0	0.008	Steel	0.54	1.53×10^{-4}
Lee et al. [14]	Closed-field unbalanced magnetron sputtering	AISI H13	19.50	32.0	8.8	0.431	Al_2O_3	0.45	–
Nainaparampil et al. [15]	Cathodic arc	M50	16.00	22.0	1.0	0.174	SUS440C	0.49	–
Akbarzadeh et al. [16]	Cathodic arc evaporation	AISI D6	13.50	22.7	7.0	0.081	WC-Co (6%)	0.60	–
CrAlN									
Ding et al. [11]	Cathodes arc deposition system	HSS	15.50	24.0	10.0	0.200	Al_2O_3	0.62	9.00×10^{-8}
Sánchez-López et al. [12]	DC magnetron sputtering	M2	20.50	28.0	5.0	0.100	Al_2O_3	0.57	–
Liu et al. [13]	Cathodic arc-evaporation	Cemented carbide	28.40	30.9	10.0	2.000	SiC	0.74	1.90×10^{-6}
Lv et al. [17]	Mid-frequency magnetron sputtering	1Cr18Mn8Ni5N	14.50	14.7	5.0	0.023	Al_2O_3	0.33	–
Lin et al. [18]	Closed-field unbalanced magnetron sputtering	AISI 304	14.60	12.9	3.0	0.020	WC-Co (6%)	0.51	9.26×10^{-6}

adhesive layer with a thickness of 200 nm. Afterwards, all of the coatings were deposited in a mixed gas of Ar and N_2 for 2 h, but the selection of the sputtering targets (Cr, Al and Ti) depended on the category of coatings. During deposition, the rotating speed of turning stage, bias voltage and optical emission monitor (OEM) were kept constant at 10 rpm, −60 V and 50%, respectively. The sputtering current of Cr target was 4.0 A whilst that of Ti and Al targets was 8.0 A.

2.2. Characterization of microstructure and mechanical properties

The crystal condition of the CrN, CrTiN, CrAlN and CrTiAlN coatings was characterized by X-ray diffraction spectra with a Cu Kα radiation (λ = 0.15404 nm) under 40 kV and 40 mA (D8-Advance, Bruker, Germany). 2θ data were recorded from 20° to 90° at a constant scanning rate of 10°/min. The chemical composition of coatings was analyzed by a scanning electron microscope with an additional EDS (FEI-SIRION 200). A white-light interferometer with Gaussian filter (cut-off length 0.08 mm) was used to measure the average roughness (Ra) (CCI 3D, Taylor Hobson Ltd. UK). Moreover, a nanoindentation (ENT-1100a, Elionix Co. Ltd.) equipped with a diamond Berkovich indenter was used to evaluate their mechanical properties. In order to minimize substrate effect and ensure the reliability of data, 120 nm (less than 6% of coatings thickness) was chosen as the penetration depth, whilst 36 nanoindentations were conducted on each coating. After test, the average values of hardness and elastic modulus with respective standard deviation were calculated. According to the Stoney's equation, which has been described in reference [19], the residual stress (σ) of each coating was calculated, and the results of mechanical properties are tabulated in Table 2.

2.3. Fracture toughness and adhesive strength

According to our previous experience, a load of 1000 mN was applied on each coating to ensure the formation of radial crack. Subsequently, the morphology of indent as well as the length of radial crack was observed via a field-emission scanning electron microscope (JEOL-JSM-7001F, Japan). Then, fracture toughness (K_{Ic}) could be obtained via Eq. (1) [20–22]:

$$K_{Ic} = \alpha\left(\frac{E}{H}\right)^{0.5}\left(\frac{P}{C_m^{1.5}}\right) \quad (1)$$

where P is load, and H and E are the hardness and elastic modulus of coatings under the same load. α is a geometric coefficient (0.016 for Berkovich indenter), whilst C_m is a mean value by averaging the lengths of 15 radial cracks. Because each impression had three radial cracks along three corners, and five nanoindentations were carried out for each sample. However, even under 1000 mN, no radial crack emanated from the impression corner of the CrTiAlN coating, and therefore, no specific value of K_{Ic} for the CrTiAlN coating is given in this study.

The adhesive strength of coatings was evaluated using micro-scratch test (WS-2005, Lanzhou institute of chemical physics, China) with a diamond tip (R = 0.2 mm and tape angle 120°). The maximum load, loading rate and scratch distance were set at 30 N, 30 N/min and 3 mm, respectively. After test, two critical loads could be confirmed via the morphology of the scratch observed by an optical microscope (XJZ-6). One is the L_{c1} as the crack initiates whilst another is the L_{c2} as the coatings delamination occurs. Laugier [23] and Bull et al. [24] defined the surface energy of an interfacial crack decades ago by using Griffith energy balance approach, and this definition has been adopted in many researchers' works [25–27] by Eq. (2):

$$G_c = \frac{\sigma_c^2 t}{2E_f} \quad (2)$$

where t and E_f are the thickness and elastic modulus of coatings, σ_c is the critical stress for coatings delamination from substrate, which could be calculated by Eq. (3):

$$\sigma_c = \left(\frac{2L_{c2}}{\pi d_c^2}\right)\left[\frac{(4+\nu_f)3\pi\mu}{8} - (1-2\nu_f)\right] \quad (3)$$

Table 2
Mechanical properties of CrN, CrTiN, CrAlN and CrTiAlN coatings.

Coatings	Thickness (μm)	H (GPa)	SD_H (GPa)	E (GPa)	E_c/E_s	H/E	H^3/E^2 (GPa)	W_e (%)	σ (GPa)	h_{max}/t
CrN	2.86	14.5	2.6	271	1.37	0.054	0.042	53.3	−2.11	1.04
CrTiN	2.95	13.9	2.1	295	1.49	0.047	0.031	48.3	−1.88	0.63
CrAlN	3.45	17.7	1.9	315	1.59	0.056	0.056	57.3	−1.80	0.58
CrTiAlN	2.05	22.0	1.4	322	1.63	0.068	0.103	63.2	−4.64	0.92

where L_{c2} and d_c are the critical load and track width as the delamination occurs; μ is the friction coefficient calculated from the friction force; while ν_f is the Poisson rate of individual coatings extracted from previous references [28–31].

3. Results and discussion

3.1. Microstructure characterization

Because of the same sputtering current (8.0 A) on Ti and Al targets, the CrTiN and CrAlN coatings exhibit a similar concentration of Ti (4.69 at.%) and Al (4.18 at.%), and the same result can be found in the CrTiAlN coating (Ti with 3.47 at.%, Al with 3.23 at.%).

As seen in Fig. 1, the CrN coating presents an F.C.C. crystal structure accompanying with Cr (110) and Cr (200) orientations originating from the adhesive layer (JCPDS 11-0065, JCPDS 06-0694). After Ti doping, a sharp CrN (111) orientation appears, and a $TiN_{0.3}$ (004) orientation around 79.5° is detected (JCPDS 41-1352). In the same way, a weak AlN (222) orientation as well as CrN (111) is found in the diffractogram of the CrAlN coating (JCPDS 46-1200). According to the previous literature, the activity of metals Cr, Al and Ti is arranged as Al > Ti > Cr [32,33]. Hence, $TiN_{0.3}$ (004) and AlN (222) form in the CrTiN and CrAlN coatings even with a low doping concentration. Since the inhibition effect on the growth of CrN (220) by Ti and Al doping, CrN (220) orientation disappears from the diffractogram of the CrTiAlN coating, but $TiN_{0.3}$ (004) and AlN (222) orientations still exist.

Even with the new formations of $TiN_{0.3}$ (004) and AlN (222), there is no big difference in the morphology amongst the CrN, CrTiN and CrAlN coatings, i.e., all of them present distinct and consecutive boundaries in Fig. 2. In contrast, the CrTiAlN coating exhibits some short seams rather than clear boundaries. Accordingly, the CrN coating exhibits the highest Ra of 1.38 nm, while the CrTiN and CrAlN coatings present the lower Ra of 0.90 nm and 0.66 nm, respectively. When Ti and Al are incorporated into the CrN coating, the beneficial effect on Ra increases and the value of the CrTiAlN coating reaches 0.48 nm as a result. Certainly, from another point of view, the most compact morphology of the CrTiAlN coating contributes to its lowest Ra to a certain extent.

3.2. Mechanical properties

As listed in Table 2, the CrAlN coating exhibits a higher hardness of 17.7 GPa while the CrTiN coating presents a lower value of 13.9 GPa than CrN coating (14.5 GPa). Since all of the plastic zone beneath the indenter should be well confined within coatings based on the penetration depth (120 nm), which is at least less than 6% of the coatings thickness [34]. The impact of thickness on hardness assessment is small enough to be ignored. From the point of the view of materials science, Ti and Al elements exist in the CrTiN and CrAlN coatings as compounds $TiN_{0.3}$ and AlN, which possibly determine the variation of their hardness. In terms of the nature of CrN, TiN and AlN crystals, all of them are covalent characters, and the individual chemical bonding energies of Al–N, Cr–N and Ti–N bonds are 297 ± 96 kJ mol^{-1}, 377.8 ± 18.8 kJ mol^{-1} and 476.1 ± 33.1 kJ mol^{-1}, respectively [35]. Consequently, the atoms in TiN are more difficult to be separated than those in CrN followed by AlN. Namely, the general order of hardness for these three crystals is TiN > CrN > AlN. Thus, the hardness of the CrTiN coating should be higher than that of the CrN coating due to the formation of TiN, while the hardness of the CrAlN should be lower as the formation of AlN. However, the results here are opposite, and hence there should be another reason to determine the tendency of hardness. According to the Scherrer's formula, the grain size of each coating can be obtained [36]:

$$D_{(hkl)} = \frac{k\lambda}{\beta\cos\theta} \tag{4}$$

where D is the average thickness of the crystal in a direction normal to the diffracting plane hkl, and k is a Scherrer constant with 0.89; λ is the wavelength of X-ray (0.15404 nm); β is the Full Width at Half Maximum (FWHM) in radian and θ is diffraction angle. The grain sizes of the CrN, CrTiN and CrAlN coatings calculated from CrN (220) are 5.98 nm, 6.84 nm and 5.13 nm. Consequently, the CrTiN coating presents a lower hardness than the CrN coating while the CrAlN coating exhibits a higher hardness due to the Hall–Petch effect [37,38]. Regarding to the CrTiAlN coating, the highest hardness of 22.0 GPa is closely related to its phase condition that the diffraction peak of CrN (220) disappears while the intensity of CrN (200) increases. Because the coatings with stronger CrN (200) and weaker CrN (220) orientations exhibited a higher hardness in the previous literature [39,40]. Moreover, the compactness of the CrTiAlN coating and the effect of stress hardening are another two contributors to its hardness [41].

In order to more clearly illustrate, only eleven load–unload curves of each coating are shown in Fig. 3. Obviously, the load–unload curves of the CrN coating scatter greatly while those of the CrTiN and CrAlN coatings shrink in some degree. As for the CrTiAlN coating, the load–unload curves from different points are almost overlapped. Through calculation, the standard deviation of hardness (SD_H) is listed in Table 2, and a decreasing tendency from 2.6 GPa to 1.4 GPa is found by Ti, Al and Ti–Al doping. There are two reasons contributing to this variation, one is the defect nature of coatings themselves during deposition while another is the Ra of coatings, which exhibits the same tendency as SD_H.

In essence, the mechanical properties of a material should be evaluated by its hardness and elastic modulus simultaneously. Thus, some researchers have suggested using the ratios of H/E and H^3/E^2 as they reflect elastic strain to failure and plastic deformation resistance of a material [42]. As the values listed in Table 2, H/E and H^3/E^2 present the same variation trend as hardness. Moreover, the elastic recovery (W_e), which was calculated through dividing recovery displacement (h_{max}-h_f) by maximum displacement (h_{max}), turns out to be the same tendency as H, H/E and H^3/E^2. Thus, taking into account H, H/E, H^3/E^2 and W_e, the CrTiAlN coating should perform the strongest crack resistance, instead, the CrTiN coating may present the poorest crack resistance even worse than CrN coating.

Regarding to the residual stress, the thickest CrAlN coatings presents the lowest residual stress (−1.80 GPa) whilst the thinnest CrAlTiN coatings shows the highest residual stress (−4.64 GPa). Generally, because of the physical constraint by the adhesion between film and substrate, a strain can be caused by the differences between their thermal expansion coefficients [43]. Subsequently, a lower residual stress is obtained when this strain is undertaken by a thick coating. The similar results have been reported in many studies [44,45].

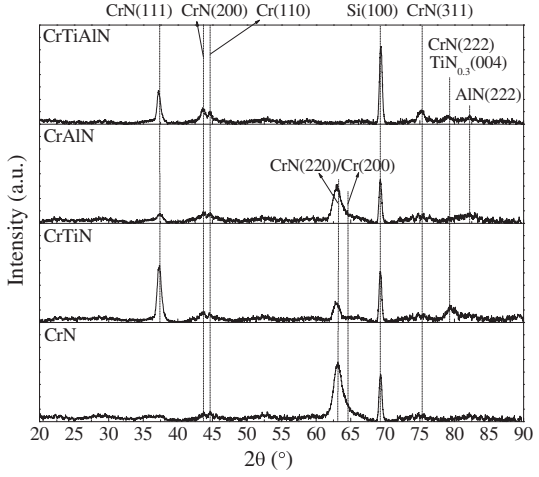

Fig. 1. XRD spectra of CrN, CrTiN, CrAlN and CrTiAlN coatings.

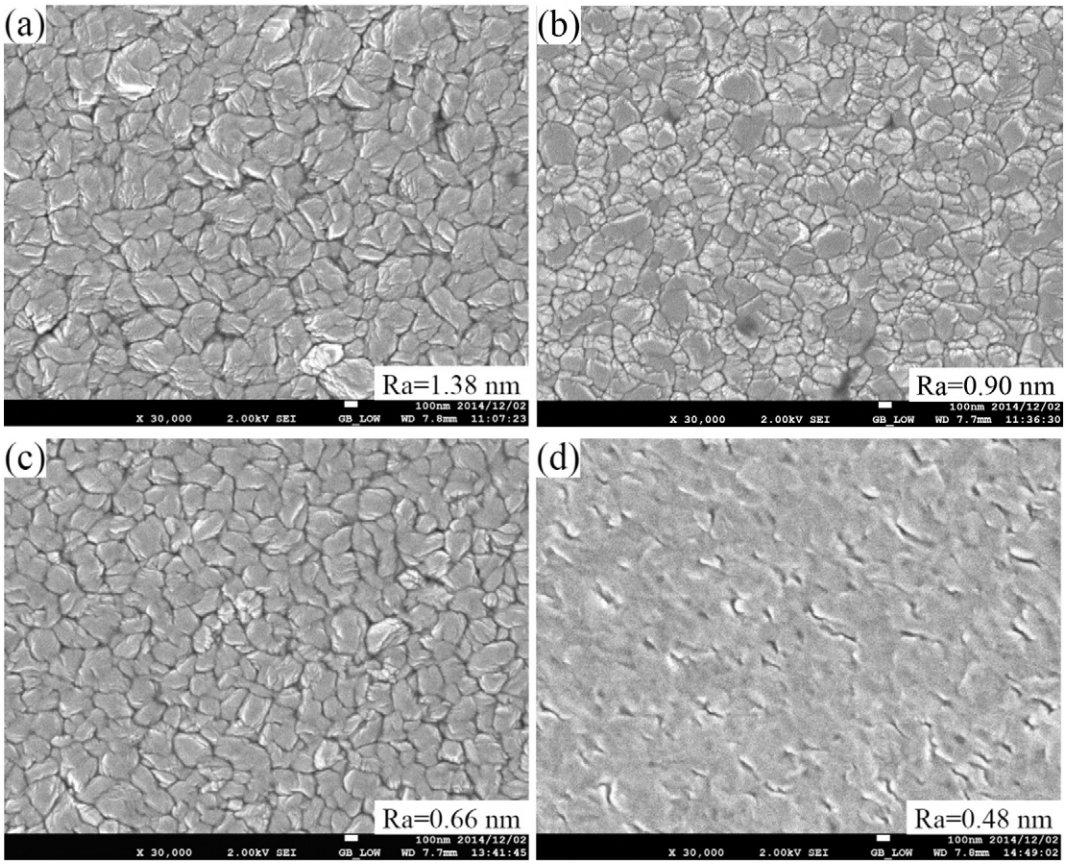

Fig. 2. Surface morphology of (a) CrN (b) CrTiN (c) CrAlN (d) CrTiAlN coatings.

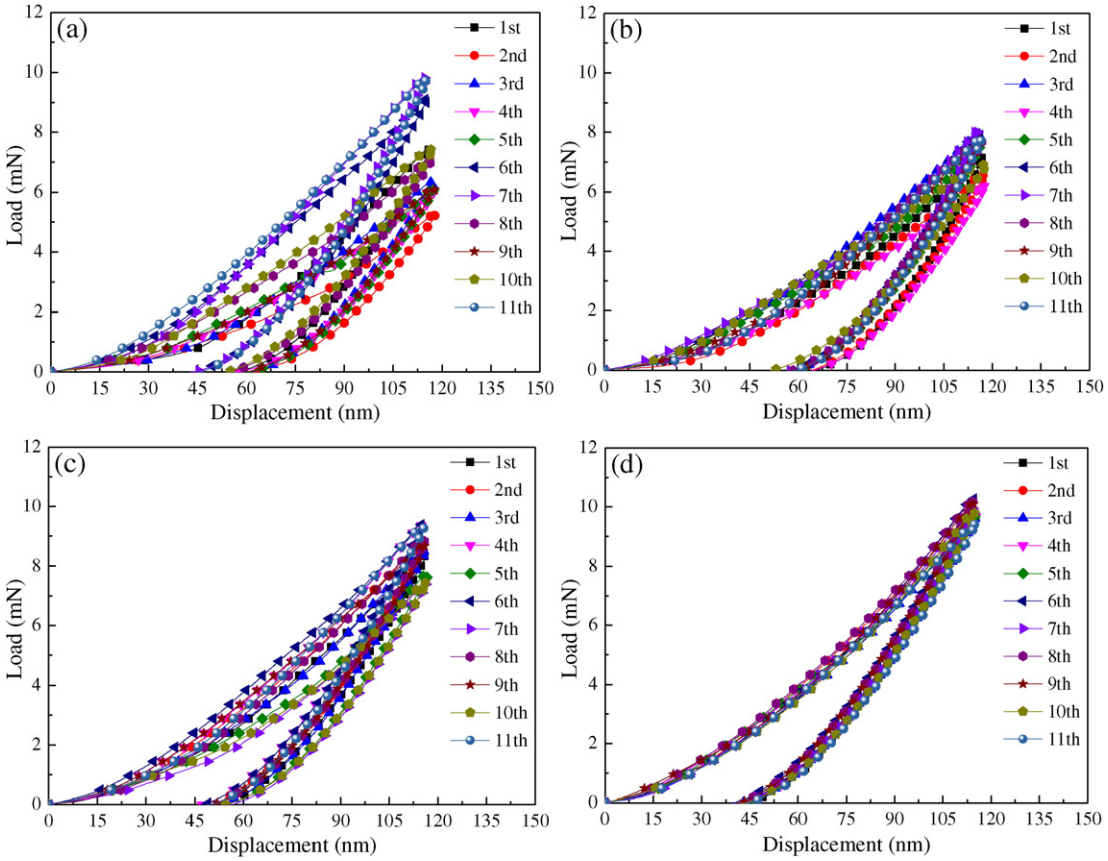

Fig. 3. Load–unload curves of (a) CrN (b) CrTiN (c) CrAlN and (d) CrTiAlN coatings at eleven locations.

3.3. Fracture toughness and crack category

The morphology of impression overviews and their corners on the CrN, CrTiN, CrAlN and CrTiAlN coatings are illustrated in Figs. 4 and 5. It is quite clear that no radial crack is found on the CrTiAlN coating, while the CrN, CrTiN and CrAlN coatings encounter the radial cracks with different lengths of 6.61, 2.51 and 2.19 μm. According to Eq. (1), the CrN coating presents the lowest fracture toughness of 1.06 MPa·$\sqrt{m}$, while the CrTiN and CrAlN coatings exhibit a higher and similar fracture toughness of 2.73 and 2.70 MPa·$\sqrt{m}$, respectively. Here, there is no specific value of fracture toughness for the CrTiAlN coating because no radial crack is found on it. Instead, two circumferential cracks are observed near the indent edge of the CrTiAlN coating in Fig. 6d. Briefly speaking, the CrN, CrTiN and CrAlN coatings encounter radial cracks while the CrTiAlN coating suffers circumferential cracks.

This phenomenon is strongly dependent on the effect of compressive stress at different locations. As seen in section A-A shown in Fig. 7, the load pressure at impression corner tends to split coatings to initiate radial cracks, but the intrinsic compressive stress of coatings inhibits this trend by a certain closing effect. Accordingly, a higher compressive stress is, a stronger inhibition effect on radial crack is. In contrast, circumferential cracks are easier to form under a higher compressive stress, because the compressive stress at impression edge makes coatings flow towards tip as shown in section B-B of Fig. 7. Subsequently, circumferential crack generates once a sufficient bending of pile-up is reached [46–48]. Thus, the high compressive stress (4.64 GPa) of the CrTiAlN coating prevents it from radial cracks but promotes the initiation of circumferential cracks. Another reflex of this high compressive stress is the pop-out that is only found on the unloading curve of the CrTiAlN coating in Fig. 8d (242 mN and 1480 nm). It is deduced that the highest compressive stress is likely to pull the material towards tip during unloading process, and extrudes the tip upwards as a spring eventually [46]. However, there was still an indenter pressure at this pop-out point (σ_{po}), and therefore, a comparison between the compressive stress (σ) and the indenter pressure at pop-out point (σ_{po}) is extremely necessary to confirm the above-mentioned deduction.

In actual condition, the real contact area should consider the elastic deflection of the material at the perimeter of indentation area [49]. Firstly, the elastic deflection at the maximum load $(h_s)_{max}$ can be obtained by Eq. (5):

$$(h_s)_{max} = \epsilon \frac{P_{max}}{S} \tag{5}$$

where ϵ is a geometrical constant equal to 0.75; P_{max} and S are the maximum load and stiffness (1005 N/mm) of the sample measured at the beginning of unloading. Then, the elastic deflection $(h_s)_i$ as well as real contact depth $(h_c)_i$ at a certain point i can be calculated by Eqs. (6) and (7) [50,51]:

$$(h_s)_i = (h_s)_{max}\sqrt{\frac{P_i}{P_{max}}} \tag{6}$$

$$(h_c)_i = h_i - (h_s)_i \tag{7}$$

where P_i and h_i are the applied load and the indenter displacement at a certain point i, respectively. Subsequently, the projected area at a certain point i during unloading process can be obtained by Eq. (8):

$$A_i = 24.5(h_c)_i^2 + \sum_{i=1}^{7} C_i (h_c)^{1/2^i} \tag{8}$$

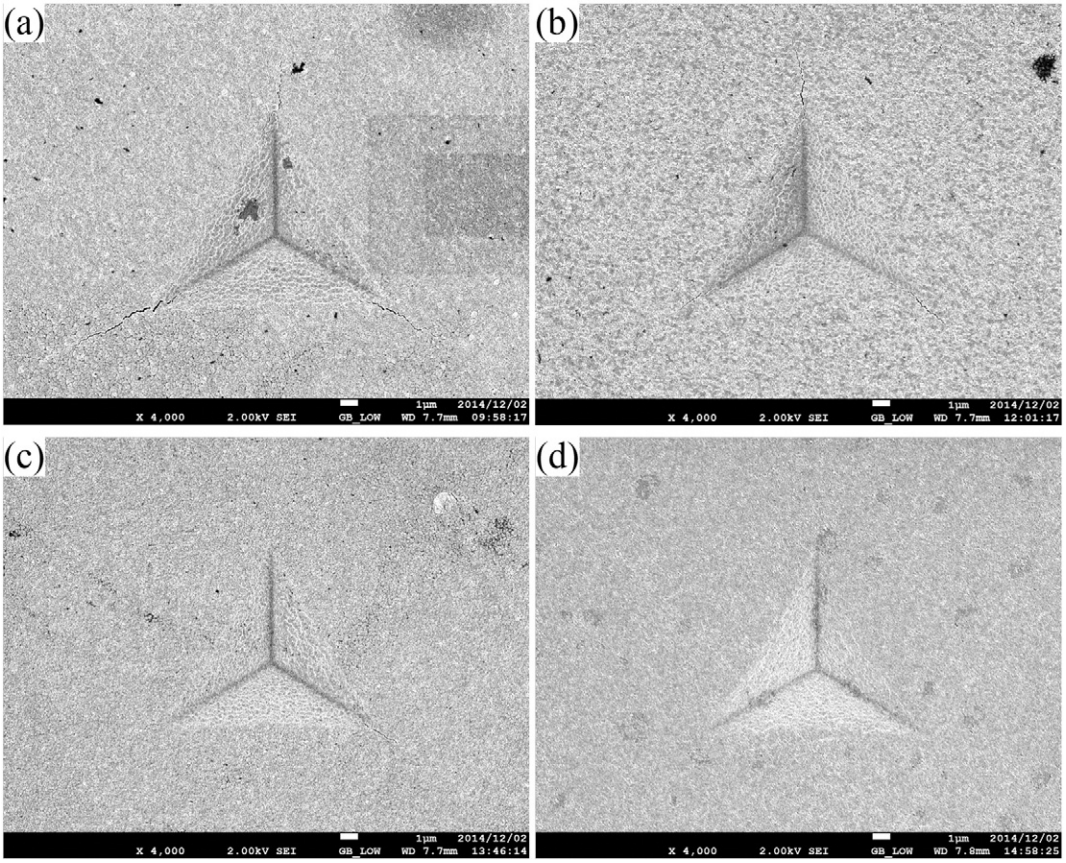

Fig. 4. Impressions of (a) CrN (b) CrTiN (c) CrAlN (d) CrTiAlN coatings after 1000 mN nanoindentation.

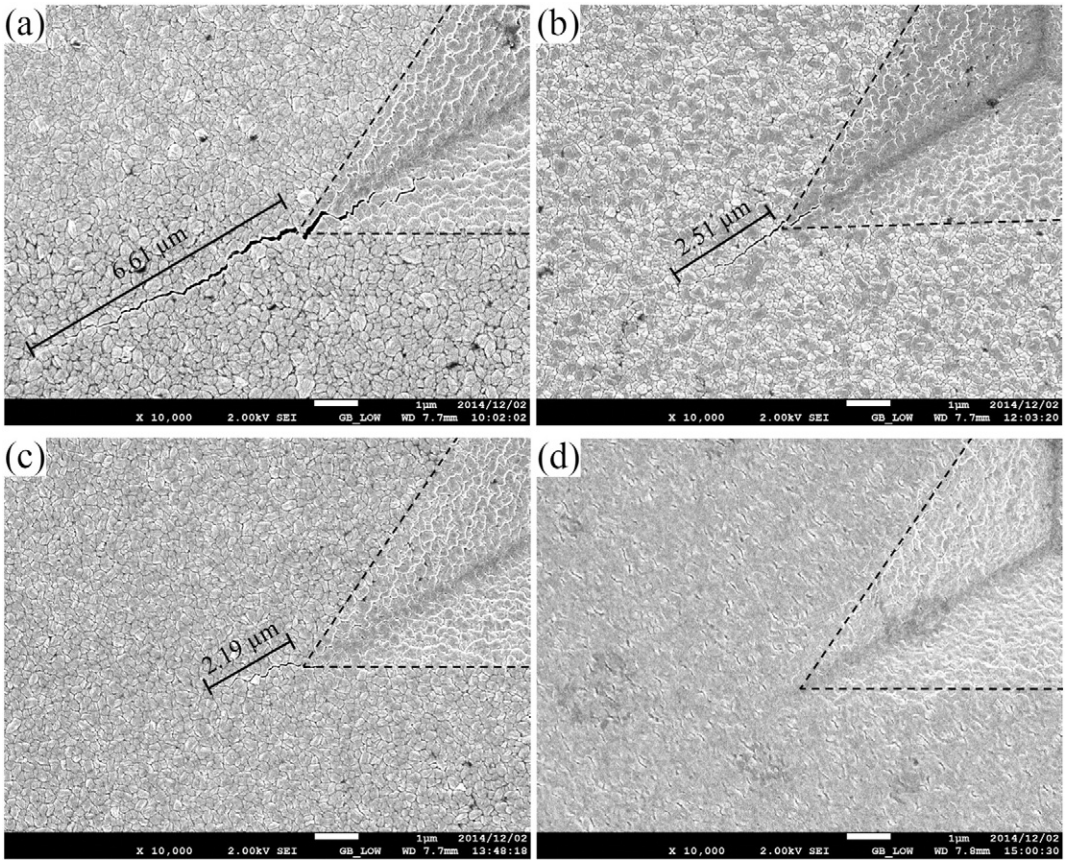

Fig. 5. Radial cracks of (a) CrN (b) CrTiN (c) CrAlN (d) CrTiAlN coatings after 1000 mN nanoindentation.

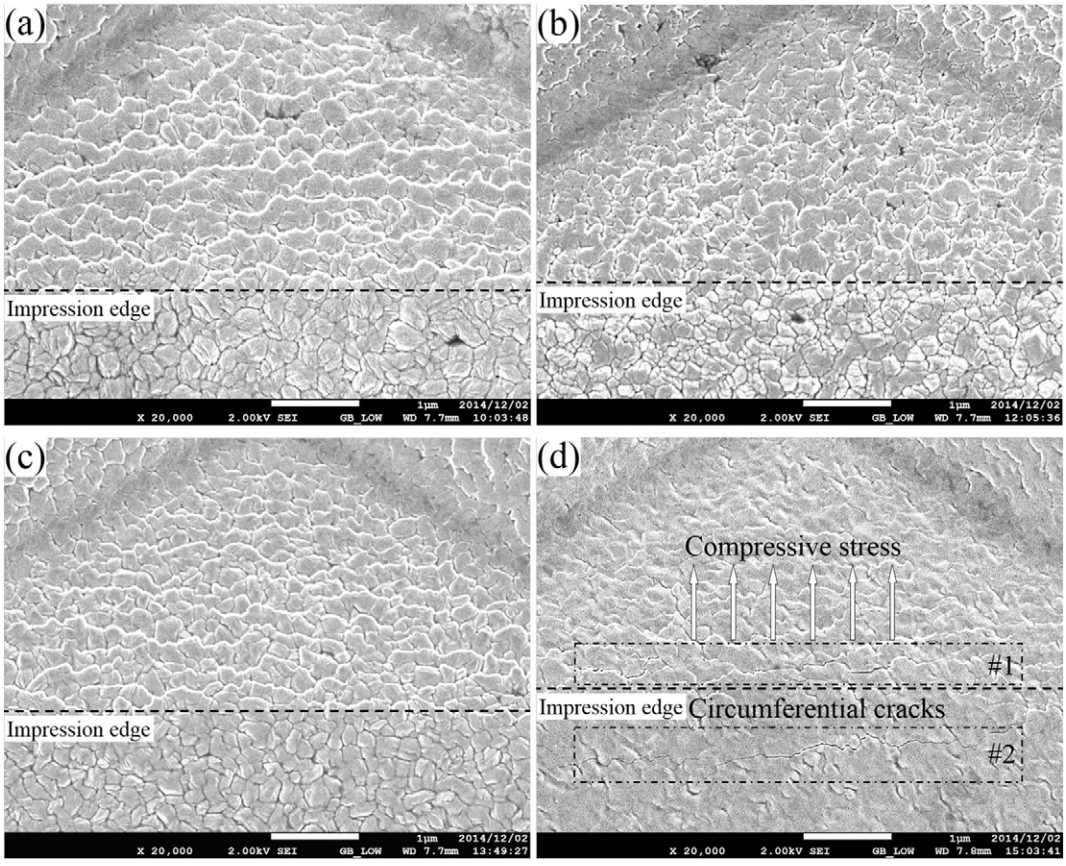

Fig. 6. Circumferential cracks of (a) CrN (b) CrTiN (c) CrAlN (d) CrTiAlN coatings after 1000 mN nanoindentation.

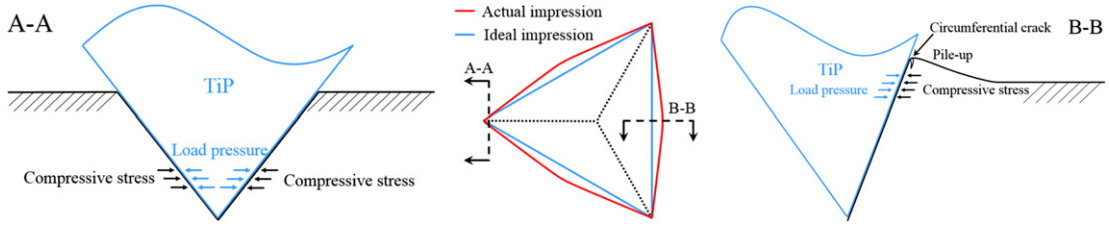

Fig. 7. Schematic diagram of effect of compressive stress at impression corner (Section A-A) and edge (Section B-B).

where C_i is a constant by experimental calibration to describe the imperfect tip geometry of Berkovich indenter.

According to the above-mentioned equations, the σ_{po} of the CrTiAlN coating at 242 mN and 1480 nm is 7.68 GPa. Obviously, the indenter pressure at pop-out point (σ_{po}) is higher than the compressive stress ($\sigma = 4.64$ GPa) of the CrTiAlN coatings. In other words, it is impossible to extrude indenter upwards indicated as a pop-out on the unloading curve.

To my knowledge, the above-mentioned equations are appropriate for sink-in condition, which means the real contact area is smaller than the theoretical contact area. However, a pile-up condition rather than sink-in is confirmed by the profile in Fig. 9a, which was scanned from the impression corner to the middle of opposite edge. Namely, the real project area (A_r surrounded by red line in Fig. 9b) is actually larger than the theoretical one (A_t surrounded by blue line in Fig. 9b), and the difference between these two areas is the project area caused by pile-up (A_p). Sullivan et al. [52] used the software ImageJ to obtain A_p, which would be calculated in this study by its length (a_i) and width (b_i) instead. According to the relation between h_i and a_i as equation below:

$$a_i = 2\sqrt{3}h_i \, tan65.27^\circ \tag{9}$$

The impression length a_i at pop-out point is 11.13 μm. After unloading, the residual width of pile-up ($b_f = 735$ nm) was extracted from the corresponding profile (Fig. 9a), but the real b_i at pop-out point should be larger than b_f, and is possibly proportional to the penetration depth as Eq. (10) [52].

$$b_i = b_f \frac{h_i}{h_f} \tag{10}$$

Thus, the b_i at pop-out is around 1014 nm where h_i and h_f are 1480 and 1072 nm, respectively. As a result, the true σ_{po} is 3.33 GPa calculated by Eq. (11).

$$\sigma_{po} = \frac{P_i}{A_r} = \frac{P_i}{(A_t + A_p)} = \frac{P_i}{24.5h_i^2 + \sum_{i=1}^{7} C_i (h_i)^{1/2^i} + 3a_i b_i/2}. \tag{11}$$

In this case, a discrepancy of 1.31 GPa is found between σ (4.64 GPa) and σ_{po} (3.33 GPa), and this led to a pop-out during unloading process. Nevertheless, there is a critical discrepancy between σ and σ_{po} for each coating, and the pop-out can be triggered only if this critical value is reached. Here, as for CrN, CrTiN and CrAlN coatings, the maximum discrepancies are 2.1 and 1.8 GPa even after complete load removing, and

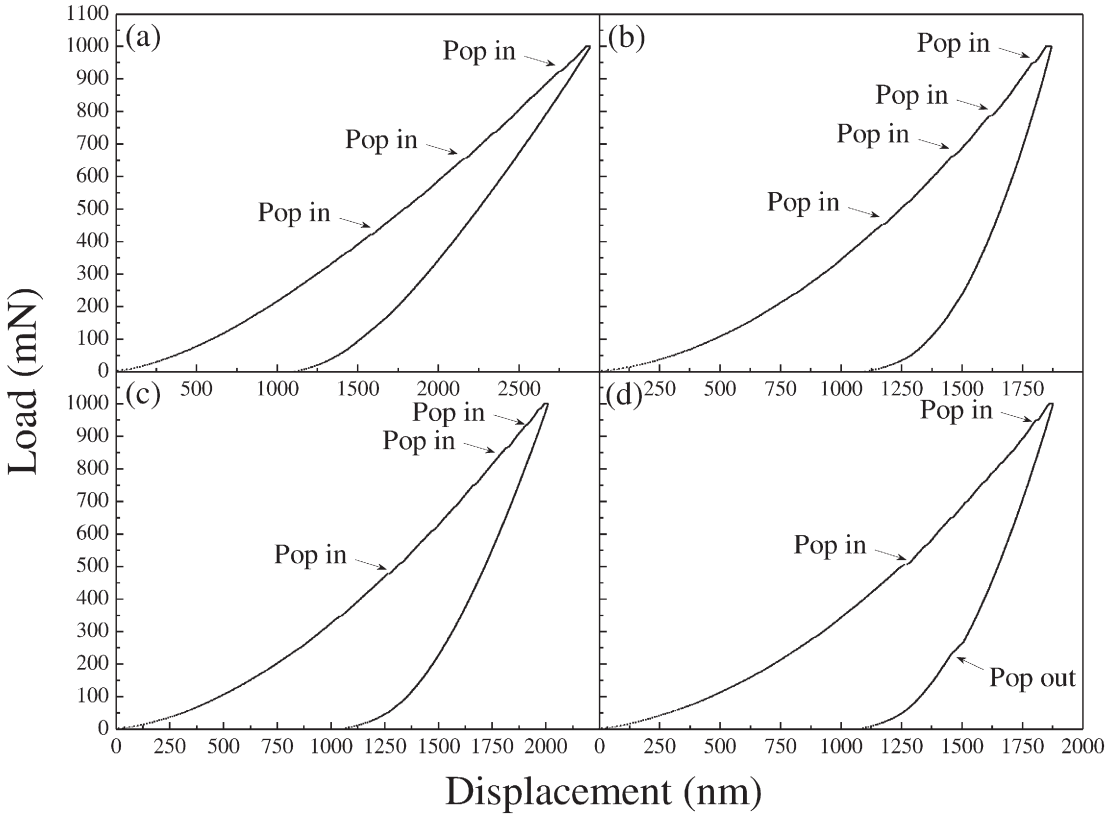

Fig. 8. Load–unload curves of (a) CrN (b) CrTiN (c) CrAlN (d) CrTiAlN coatings under 1000 mN nanoindentation.

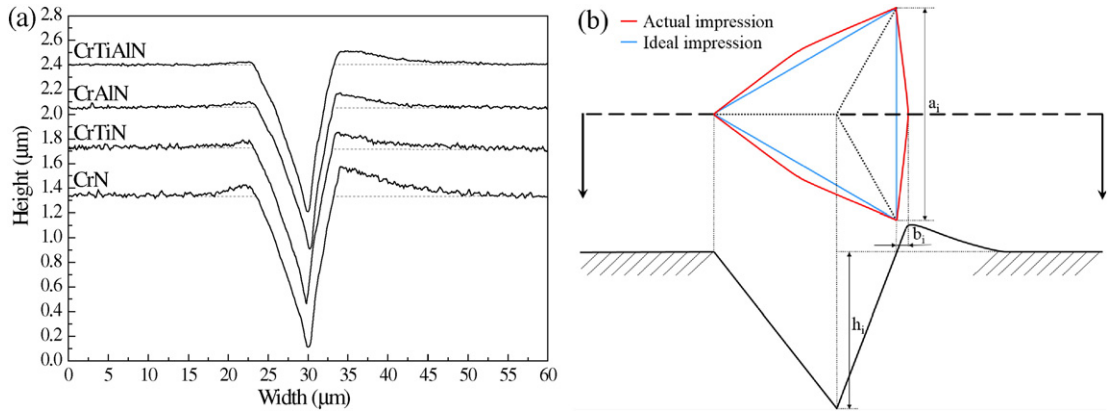

Fig. 9. (a) Contours of impressions after 1000 mN nanoindentation and (b) schematic diagram of project area under pile-up situation.

should be lower than the critical value as there is no pop-out shown on their unloading curves. Considering the compressive stress of the coatings in this study and our previous works [19,53], a decent compressive stress around 3.0 GPa is likely to help coatings prevent from radial and circumferential cracks simultaneously. However, this deduction still needs more data to support.

Subtracting the displacement of the former point from the displacement of the later one on the loading curve, an evolution of displacement difference as a function of load as well as a total distance of pop-in (d_{pi}) is shown in Fig. 10. The CrN coating exhibits the longest pop-in distance (104.5 nm) while the CrTiN and CrAlN coatings present a shorter and similar value (69.5–70.4 nm). These d_{pi} are closely associated with crack formation [54,55] and well consistent with the individual crack lengths shown in Fig. 5. However, even without any radial cracks, the CrTiAlN coating still exhibits a similar pop-in distance (70.3 nm) as those of the CrTiN and CrAlN coatings. This result is closely associated with the formation of circumferential cracks here. As seen the curve of the CrTiAlN coating in Fig. 10, two large differences of the displacement display at 506 mN and 950 mN. According to the load–unload curve in Fig. 8d and Eq. (9), the corresponding lengths of impression edges under these two loads are 9.48 μm and 13.54 μm. On the other hand, the lengths of impression edges along two circumferential cracks in Fig. 6d are around 9.8 and 13.2 μm, which can be measured in Fig. 11. It turns out that the measured lengths are very close to the calculated lengths (9.48 μm and 13.54 μm). It indicates that the CrTiAlN coating encountered the first circumferential crack at 506 mN followed by the second circumferential crack at 950 mN. Because of the elastic recovery after load removing, the final impression edge rebounds to the position that locates in the middle of two circumferential cracks as shown in Fig. 6d. Thus, these two large pop-in distances at 506 mN and 950 mN for the CrTiAlN coating definitely result from the formation of circumferential cracks. If these two pop-in distances are omitted, the total pop-in distance for the CrTiAlN coating is around 47.8 nm, which will be the lowest value. From another point of view, it implies that the CrTiAlN coating presents the best resistance to radial crack.

Besides mechanical properties, elastic recovery (W_e) and residual stress of coatings themselves, the properties of substrate (H_s and E_s) play an important role in determining the fracture toughness. Musil et al. [56,57] pointed out the different effects between 'soft substrate' and 'hard substrate', but all of the coatings here have a higher hardness (13.9–22.0 GPa) than Si (100) substrate (12.4 GPa), i.e., all of the toughness are assessed under the same condition of 'soft substrate'. On the other hand, according to reference [58], the necessary condition to avoid film cracking is of a little bit higher modulus ratio ($E_c/E_s \geq 1.3$), and the higher of this value is, the stronger crack inhibition is. Consequently, the CrTiAlN coating with the highest E_c/E_s (1.63) presents the strongest resistance to radial cracks.

The last but not the least, penetration depth (h_{max}) close to or even over the thickness of coatings (t) makes the radial crack occur easily [57]. Thus, the highest h_{max}/t of the CrN coating leads to its longest radial crack as well. On the contrary, even with a higher h_{max}/t than that of the CrTiN and CrAlN coatings, no radial crack is found along impression corner of the CrTiAlN coating. It demonstrates the strongest radial crack resistance of the CrTiAlN coating from another perspective.

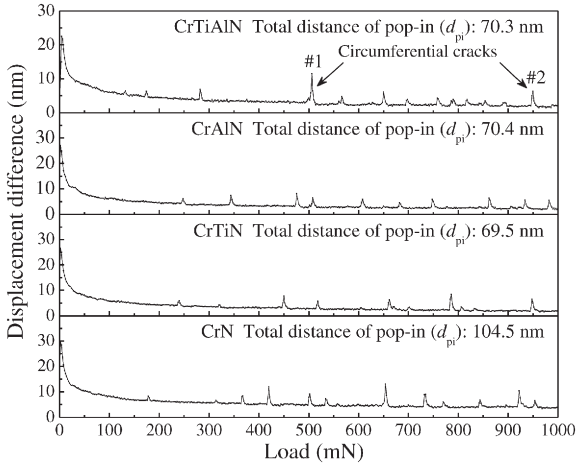

Fig. 10. Evolution of displacement difference as a function of load for CrN, CrTiN, CrAlN and CrTiAlN coatings.

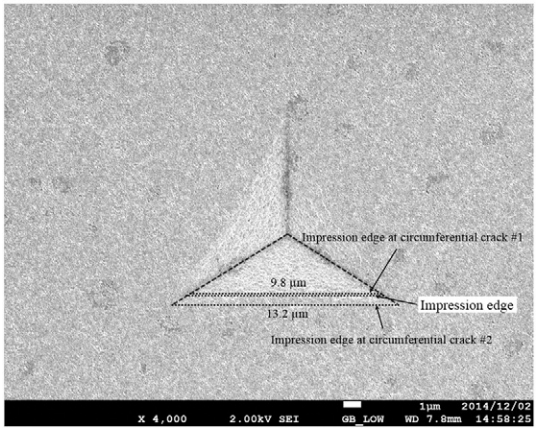

Fig. 11. Corresponding lengths of impression edges at occurrence of circumferential crack #1 and #2 on CrTiAlN coating.

3.4. Adhesive energy

The critical loads of crack initiation (L_{c1}) and coatings delamination (L_{c2}) were extracted from the optical images of whole scratch and crack initiation, which are illustrated in Fig. 12. As listed in Table 3, L_{c1} just varies in a range of 12.7 to 13.4 N for the CrN, CrTiN and CrAlN coatings while the L_{c1} of the CrTiAlN coating reaches up to 17.1 N. According to the definition of L_{c1}, the CrTiAlN demonstrates its strongest crack resistance from another perspective. However, L_{c2} shows a different tendency from L_{c1}. A lowest value of 17.5 N is obtained for the CrTiAlN coating while the CrTiN coating presents the highest L_{c2} of 28.2 N. Based on Eqs. (2) and (3), the individual critical stress and adhesive energy for each coating are listed in Table 3. It is obvious that, after taking in account the elastic modulus and thickness of coatings, the CrAlN rather than CrTiN coating demonstrates the highest adhesive energy of 313 J/m^2 while the CrTiAlN coating still exhibits the lowest value of 70 J/m^2. Importantly, the adhesive energy of each coating is well consistent with its compressive stress.

4. Conclusions

The mechanical properties, crack resistance and adhesive strength of the CrN, CrTiN, CrAlN and CrTiAlN coatings were evaluated via nanoindentation and micro-scratch tests. In addition, the fracture toughness and adhesive energy of each coating were calculated. Conclusions are drawn as follows:

(1) Besides an F.C.C. crystal structure of CrN, $TiN_{0.3}$ and AlN phases generated in the CrTiN, CrAlN and CrTiAlN coatings.
(2) The CrAlN coating exhibited a higher hardness of 17.7 GPa while the CrTiN coating presented a lower hardness of 13.9 GPa than

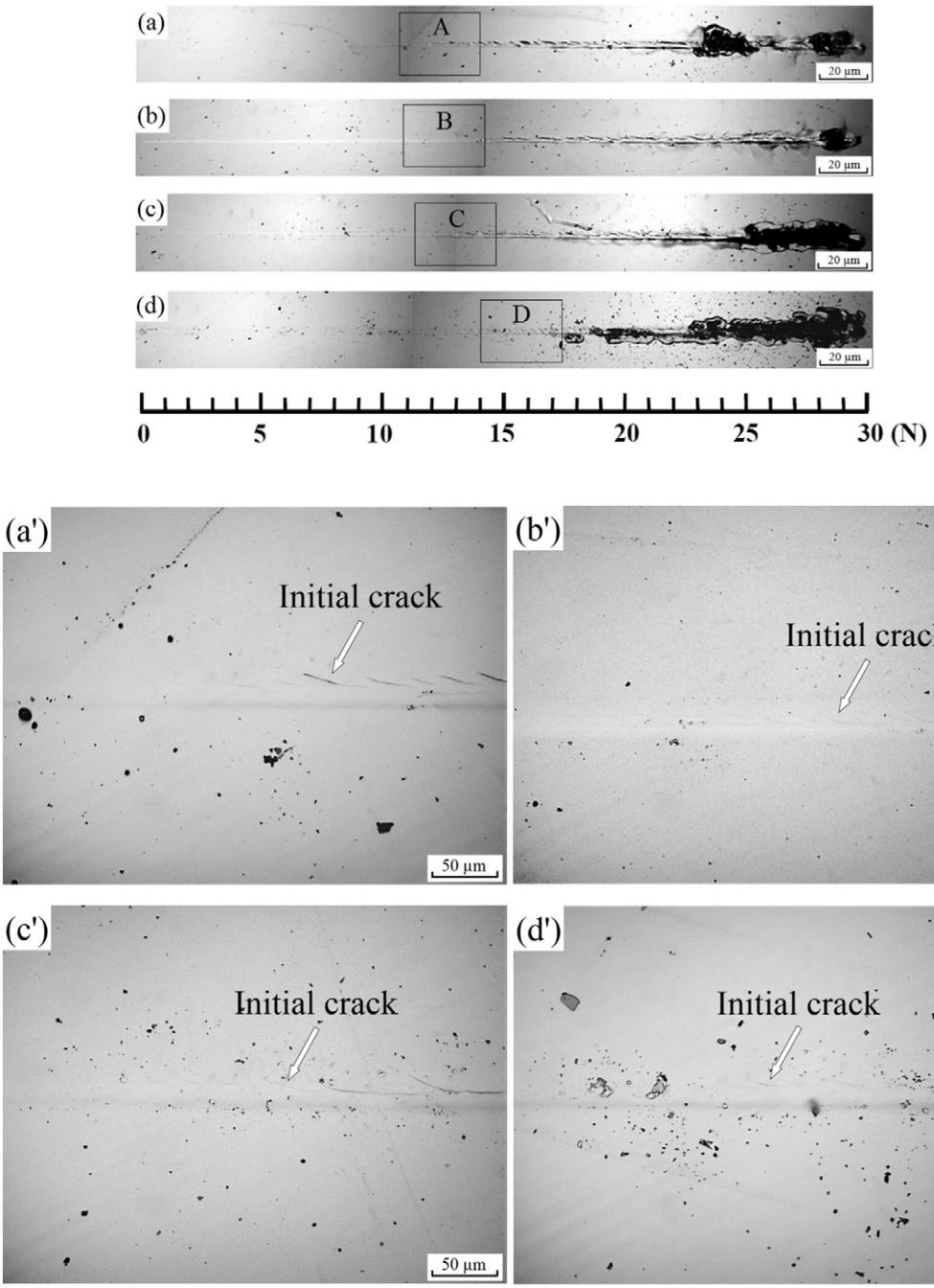

Fig. 12. Scratch morphology of (a) CrN (b) CrTiN (c) CrAlN (d) CrTiAlN coatings and enlarged areas (a') Area A (b') Area B (c') Area C (d') Area D.

Table 3
Critical load, critical stress, adhesion energy and fracture toughness of CrN, CrTiN, CrAlN and CrTiAlN coatings.

Coatings	ν	μ	L_{c1} (N)	L_{c2} (N)	σ_c (GPa)	G_c (J/m^2)	C_m (μm)	K_{Ic} (MPa·$\sqrt{m}$)
CrN	0.20[a]	0.051	12.7	23.2	5.3	150	11.86	1.06
CrTiN	0.22[b]	0.053	13.0	28.2	5.8	168	10.02	2.73
CrAlN	0.25[c]	0.053	13.4	24.9	7.6	313	8.52	2.70
CrTiAlN	0.23[d]	0.032	17.1	17.5	4.7	70	–	No radial crack

[a] The Poisson rate (ν) of CrN coatings is obtained from Ref. [28].
[b] The Poisson rate (ν) of CrTiN coatings is obtained from Ref. [29].
[c] The Poisson rate (ν) of CrAlN coatings is obtained from Ref. [30].
[d] The Poisson rate (ν) of CrTiAlN coatings is obtained from Ref. [31].

the CrN coating (14.5 GPa) due to the Hall–Petch effect. A relatively intensive CrN(200) orientation and compactness contributed to the highest hardness (22.0 GPa) of the CrTiAlN coating.

(3) The CrTiAlN coating presented the strongest resistance to radial cracks while the CrN coating exhibited the weakest fracture toughness (1.06 MPa·$\sqrt{m}$). Ternary CrTiN and CrAlN coatings showed an intermediate fracture toughness with a similar value around 2.70 MPa·$\sqrt{m}$.

(4) The CrTiAlN coating encountered circumferential cracks with a pop-out on unloading curve, and presented the lowest adhesive strength (70 J/m^2) due to the highest compressive stress (4.64 GPa).

(5) A decent compressive stress (3.0 GPa) is of paramount importance to avoid radial and circumferential cracks simultaneously.

Acknowledgements

This work has been initiated by a Japan–China joint research project and partially supported by a research grant from Keio Leading-edge Laboratory of Science and Technology (KLL) in Keio University. This work has been also supported by National Natural Science Foundation of China (Grant No. 51375231), Research Fund for Doctoral Program of Higher Education (Grant No.20133218110030) and Project Funded by Priority Academic Program Development of Jiangsu Higher Education Institutions (PAPD). We would like to acknowledge them for their financial support.

Appendix A. Supplementary data

Supplementary data to this article can be found online at http://dx.doi.org/10.1016/j.surfcoat.2015.11.040.

References

[1] H.C. Barshilia, N. Selvakumar, B. Deepthi, K.S. Rajam, A comparative study of reactive direct current magnetron sputtered CrAlN and CrN coatings, Surf. Coat. Technol. 201 (2006) 2193–2201.
[2] S.R. Pulugurtha, D.G. Bhat, M.H. Gordon, J. Shultz, M. Staia, S.V. Joshi, S. Govindarajan, Mechanical and tribological properties of compositionally graded CrAlN films deposited by AC reactive magnetron sputtering, Surf. Coat. Technol. 202 (2007) 1160–1166.
[3] Y.C. Chim, X.Z. Ding, X.T. Zeng, S. Zhang, Oxidation resistance of TiN, CrN, TiAlN and CrAlN coatings deposited by lateral rotating cathode arc, Thin Solid Films 517 (2009) 4845–4849.
[4] X.T. Zeng, S. Zhang, J. Hsieh, Development of graded Cr-Ti-N coatings, Surf. Coat. Technol. 102 (1998) 108–112.
[5] M.A. Ezazi, M.M. Quazi, E. Zalnezhad, A.A.D. Sarhan, Enhancing the tribo-mechanical properties of aerospace AL7075-T6 by magnetron-sputtered Ti/TiN, Cr/CrN & TiCr/TiCrN thin film ceramic coatings, Ceram. Int. 40 (2014) 15603–15615.
[6] G.A. Zhang, P.X. Yan, P. Wang, Y.M. Chen, J.Y. Zhang, The structure and tribological behaviors of CrN and Cr-Ti-N coatings, Appl. Surf. Sci. 253 (2007) 7353–7359.
[7] C.H. Hsu, K.L. Chen, Z.H. Lin, C.Y. Su, C.K. Lin, Bias effects on the tribological behavior of cathodic arc evaporated CrTiAlN coatings on AISI 304 stainless steel, Thin Solid Films 518 (2010) 3825–3829.
[8] L. Lu, Q.M. Wang, B.Z. Cheng, Y.C. Ao, D.H. Yu, C.Y. Wang, S.H. Wu, K.H. Kim, Microstructure and cutting performance of CrTiAlN coating for high-speed dry milling, Trans. Nonferrous Metals Soc. China 24 (2014) 1800–1806.
[9] Q. Yang, L.R. Zhao, F. Cai, S. Yang, D.G. Teer, Wear, erosion and corrosion resistance of CrTiAlN coating deposited by magnetron sputtering, Surf. Coat. Technol. 202 (2008) 3886–3892.
[10] Q. Yang, F. Cai, L.R. Zhao, X. Huang, Improving corrosion resistance of CrTiAlN coating by post-deposition treatments, Surf. Coat. Technol. 203 (2008) 606–609.
[11] X.Z. Ding, X.T. Zeng, Y.C. Liu, F.Z. Fang, G.C. Lim, $Cr_{1-x}Al_xN$ coatings deposited by lateral rotating cathode arc for high speed machining applications, Thin Solid Films 516 (2008) 1710–1715.
[12] J.C. Sánchez-López, A. Contreras, S. Domínguez-Meister, A. García-Luis, M. Brizuela, Tribological behaviour at high temperature of hard CrAlN coatings doped with Y or Zr, Thin Solid Films 550 (2014) 413–420.
[13] A.H. Liu, J.X. Deng, H.B. Cui, Y.Y. Chen, J. Zhao, Friction and wear properties of TiN, TiAlN, AlTiN and CrAlN PVD nitride coatings, Int. J. Refract. Met. Hard Mater. 31 (2012) 82–88.
[14] S.Y. Lee, G.S. Kim, J.H. Hahn, Effect of the Cr content on the mechanical properties of nanostructured TiN/CrN coatings, Surf. Coat. Technol. 177–178 (2004) 426–433.
[15] J.J. Nainaparampil, J.S. Zabinski, A. Korenyi-Both, Formation and characterization of multiphase film properties of (Ti–Cr)N formed by cathodic arc deposition, Thin Solid Films 333 (1998) 88–94.
[16] M. Akbarzadeh, A. Shafyei, H.R. Salimijazi, Characterization of TiN, CrN and (Ti, Cr)N coatings deposited by cathodic arc evaporation, Int. J. Eng. Trans. A 27 (2014) 1127–1132.
[17] Y.H. Lv, L. Ji, X.H. Liu, H.X. Li, H.D. Zhou, J.M. Chen, Influence of substrate bias voltage on structure and properties of the CrAlN films deposited by unbalanced magnetron sputtering, Appl. Surf. Sci. 258 (2012) 3864–3870.
[18] J. Lin, B. Mishra, J.J. Moore, W.D. Sproul, J.A. Rees, Effects of the substrate to chamber wall distance on the structure and properties of CrAlN films deposited by pulsed-closed field unbalanced magnetron sputtering (P-CFUBMS), Surf. Coat. Technol. 201 (2007) 6960–6969.
[19] Q.Z. Wang, Z.W. Wu, F. Zhou, H. Huang, K. Niitsu, J.W. Yan, Evaluation of crack resistance of CrSiCN coatings as a function of Si concentration via nanoindentation, Surf. Coat. Technol. 272 (2015) 239–245.
[20] A.G. Evans, E.A. Charles, Fracture toughness determinations by indentation, J. Am. Ceram. Soc. 59 (7–8) (1976) 371–372.
[21] S. Zhang, X.M. Zhang, Toughness evaluation of hard coatings and thin films, Thin Solid Films 520 (2012) 2375–2389.
[22] S. Zhang, D. Sun, Y.Q. Fu, H.J. Du, Toughness measurement of thin films: a critical review, Surf. Coat. Technol. 198 (2005) 74–78.
[23] M.T. Laugier, Adhesion of TiC and TiN coatings prepared by chemical vapor deposition on WC-Co-based cemented carbides, J. Mater. Sci. 21 (1986) 2269–2272.
[24] S.J. Bull, D.S. Rickerby, New developments in the modelling of the hardness and scratch adhesion of thin films, Surf. Coat. Technol. 42 (1990) 149–164.
[25] S.Y. Chang, Y.C. Huang, Analyses of interface adhesion between porous SiO_2 low-k film and SiC/SiN layers by nanoindentation and nanoscratch tests, Microelectron. Eng. 84 (2007) 319–327.
[26] S.Y. Chang, Y.S. Lee, C.L. Lu, Effect of plasma treatments on the interface chemistry and adhesion strength between Cu metallization and SiCN etch stop layer electrochemical/chemical deposition and etching, J. Electrochem. Soc. 154 (2007) D241–D248.
[27] Y.C. Huang, S.Y. Chang, C.H. Chang, Effect of residual stresses on mechanical properties and interface adhesion strength of SiN thin films, Thin Solid Films 517 (2009) 4857–4861.
[28] A. Kondo, T. Oogami, K. Sato, Y. Tanaka, Structure and properties of cathodic arc ion plated CrN coatings for copper machining cutting tools, Surf. Coat. Technol. 177–178 (2004) 238–244.
[29] K.H. Lee, C.H. Park, Y.S. Yoon, J.J. Lee, Structure and properties of $(Ti_{1-x}Cr_x)N$ coatings produced by the ion-plating method, Thin Solid Films 385 (2001) 167–173.
[30] P.H. Mayrhofer, D. Music, T. Reeswinkel, H.G. Fuß, J.M. Schneider, Structure, elastic properties and phase stability of $Cr_{1-x}Al_xN$, Acta Mater. 56 (2008) 2469–2475.
[31] Q. Luo, A.H. Jones, High-precision determination of residual stress of polycrystalline coatings using optimised XRD-$\sin^2\psi$ technique, Surf. Coat. Technol. 205 (2010) 1403–1408.
[32] S.G. Bratsch, Standard electrode potentials and temperature coefficients in water at 298.15 K, J. Phys. Chem. Ref. Data 18 (1989) 1–21.
[33] V. Petr, Electrochemical series, in: W.M. Haynes (Ed.), Handbook of Chemistry and Physics, CRC Press, Florida 2014, pp. 80–89.
[34] X. Cai, H. Bangert, Hardness measurements of thin films—determining the critical ratio of depth to thickness using FEM, Thin Solid Films 264 (1995) 59–71.
[35] D.R. Lide (Ed.), CRC Handbook of Chemistry and Physics, CRC Press, Boca Raton, Florida, 2005.
[36] P. Scherrer, N.G.W. Gottingen, Math.-Pys. Kl. 2 (1918) 96–100.
[37] E.O. Hall, The deformation and ageing of mild steel: II characteristics of the luders deformation, Proc. Phys. Soc. London, Sect. B 64 (1951) 742–747.
[38] E.O. Hall, The deformation and ageing of mild steel: III discussion of results, Proc. Phys. Soc. London, Sect. B 64 (1951) 747–753.
[39] J.W. Lee, S.K. Tien, Y.C. Kuo, C.M. Chen, The mechanical properties evaluation of the CrN coatings deposited by the pulsed DC reactive magnetron sputtering, Surf. Coat. Technol. 200 (2006) 3330–3335.
[40] H.N. Shah, R. Jayaganthan, D. Kaur, Influence of silicon content on the microstructure and hardness of CrN coatings deposited by reactive magnetron sputtering, Mater. Chem. Phys. 121 (2010) 567–571.
[41] Y.X. Wang, S. Zhang, J.W. Lee, W.S. Lew, B. Li, Influence of bias voltage on the hardness and toughness of CrAlN coatings via magnetron sputtering, Surf. Coat. Technol. 206 (2012) 5103–5107.
[42] N.A. Sakharova, J.V. Fernandes, M.C. Oliveira, J.M. Antunes, Influence of ductile interlayers on mechanical behaviour of hard coatings under depth-sensing indentation: a numerical study on TiAlN, J. Mater. Sci. 45 (2010) 3812–3823.

[43] T.P. Kumari, M.M. Raja, A. Kumar, S. Srinath, S.V. Kamat, Effect of thickness on structure, microstructure, residual stress and soft magnetic properties of DC sputtered $Fe_{65}Co_{35}$ soft magnetic thin films, J. Magn. Magn. Mater. 365 (2014) 93–99.
[44] T. Pecnik, S. Glinsek, B. Kmet, B. Malic, Combined effects of thickness, grain size and residual stress on the dielectric properties of $Ba_{0.5}Sr_{0.5}TiO_3$ thin films, J. Alloys Compd. 646 (2015) 766–772.
[45] L.J. Gu, X.Z. Fan, Y. Zhao, B.L. Zou, Y. Wang, S.M. Zhao, X.Q. Cao, Influence of ceramic thickness on residual stress and bonding strength for plasma sprayed duplex thermal barrier coating on aluminum alloy, Surf. Coat. Technol. 206 (2012) 4403–4410.
[46] T. An, M. Wen, C.Q. Hu, H.W. Tian, W.T. Zheng, Interfacial fracture for TiN/SiN_x Nanomultilayer coatings on Si (111) characterized by nanoindentation experiments, Mater. Sci. Eng. A 494 (2008) 324–328.
[47] J. Chen, S.J. Bull, Assessment of the toughness of thin coatings using nanoindentation under displacement control, Thin Solid Films 494 (2006) 1–7.
[48] J.J. Chen, S.J. Bull, Modelling the limits of coating toughness in brittle coated systems, Thin Solid Films 517 (2009) 2945–2952.
[49] W.C. Oliver, G.M. Pharr, An improved technique for determining hardness and elastic modulus using load and displacement sensing indentation experiments, J. Mater. Res. 7 (1992) 1564–1583.
[50] I.N. Sneddon, The relation between load and penetration in the axisymmetric Boussinesq problem for a punch of arbitrary profile, Int. J. Eng. Sci. 3 (1965) 47–57.
[51] N.V. Novikov, S.N. Dub, Y.V. Milman, I.V. Gridneva, S.I. Chugunova, Application of nanoindentation method to study a semiconductor–metal phase transformation in silicon, J. Superhard Mater. 18 (1996) 32–40.
[52] M. Sullivan, B.C. Prorok, Evaluating indent pile-up with metallic films on ceramic-like substrates, J. Mater. Res. 30 (2015) 2046–2054.
[53] Q.Z. Wang, Z.W. Wu, F. Zhou, J.W. Yan, Comparison of crack resistance between ternary CrSiC and quaternary CrSiCN coatings via nanoindentation, Mater. Sci. Eng. A 642 (2015) 391–397.
[54] S.R. Jian, S.C. Jason, Jang, Berkovich nanoindentation on InP, J. Alloys Compd. 482 (2009) 498–501.
[55] C.Y. Yen, S.R. Jian, Y.S. Lai, P.F. Yang, Y.Y. Liao, J.S.C. Jang, T.H. Lin, J.Y. Juang, Mechanical properties of the hexagonal $HoMnO_3$ thin films by nanoindentation, J. Alloys Compd. 508 (2010) 523–527.
[56] M. Jirout, J. Musil, Effect of addition of Cu into ZrO_x film on its properties, Surf. Coat. Technol. 200 (2006) 6792–6800.
[57] J. Musil, M. Jirout, Toughness of hard nanostructured ceramic thin films, Surf. Coat. Technol. 201 (2007) 5148–5152.
[58] M.A. Meyers, A. Mishra, D.J. Benson, Mechanical properties of nanocrystalline materials, Prog. Mater. Sci. 51 (2006) 427–556.